View metadata, citation and similar papers at core.ac.uk
brought to you by CORE
provided by Elsevier - Publisher Connector

Chemistry & Biology
Article

Mycobacterial Phenolic Glycolipid Virulence Factor Biosynthesis: Mechanism and Small-Molecule Inhibition of Polyketide Chain Initiation

Julian A. Ferreras,[1,5] Karen L. Stirrett,[1,5] Xuequan Lu,[2] Jae-Sang Ryu,[2,6] Clifford E. Soll,[3] Derek S. Tan,[2] and Luis E.N. Quadri[1,4,*]
[1]Department of Microbiology and Immunology, Weill Medical College of Cornell University, 1300 York Avenue, New York, NY 10021, USA
[2]Molecular Pharmacology and Chemistry Program and Tri-Institutional Research Program, Memorial Sloan-Kettering Cancer Center, 1275 York Avenue, Box 422, New York, NY 10065, USA
[3]Hunter College, Chemistry Department, 695 Park Avenue, New York, NY 10021, USA
[4]Molecular Biology Program and Tri-Institutional Training Program in Chemical Biology, Weill Graduate School of Medical Sciences of Cornell University, 1300 York Avenue, New York, NY 10021, USA
[5]These authors contributed equally to this work.
[6]Present address: College of Pharmacy, A-208, Ewha Womans University, 11-1 Daehyun-dong, Seodaemun-gu, Seoul, 120-750, Korea.
*Correspondence: leq2001@med.cornell.edu
DOI 10.1016/j.chembiol.2007.11.010

SUMMARY

Phenolic glycolipids (PGLs) are polyketide-derived virulence factors produced by *Mycobacterium tuberculosis*, *M. leprae*, and other mycobacterial pathogens. We have combined bioinformatic, genetic, biochemical, and chemical biology approaches to illuminate the mechanism of chain initiation required for assembly of the *p*-hydroxyphenyl-polyketide moiety of PGLs. Our studies have led to the identification of a stand-alone, didomain initiation module, FadD22, comprised of a *p*-hydroxybenzoic acid adenylation domain and an aroyl carrier protein domain. FadD22 forms an acyl-*S*-enzyme covalent intermediate in the *p*-hydroxyphenyl-polyketide chain assembly line. We also used this information to develop a small-molecule inhibitor of PGL biosynthesis. Overall, these studies provide insights into the biosynthesis of an important group of small-molecule mycobacterial virulence factors and support the feasibility of targeting PGL biosynthesis to develop new drugs to treat mycobacterial infections.

INTRODUCTION

Mycobacterium tuberculosis and *M. leprae*, the etiologic agents of tuberculosis and leprosy, respectively, are pathogens with serious impacts on global public health (World Health Organization, 2007a, 2007b). Tuberculosis is one of the top ten leading causes of death in the world and is responsible for nearly two million deaths per year. Moreover, the growing incidence of multidrug-resistant (MDR) tuberculosis and the emergence of extensively/extremely drug-resistant strains pose a new threat (Aziz et al., 2006; Centers for Disease Control and Prevention, 2006). Although leprosy has been controlled effectively using multidrug therapy, it remains one of the major causes of nontraumatic neuropathy, and there are over three million people with leprosy-derived disabilities worldwide (Agrawal et al., 2005; Britton and Lockwood, 2004). Furthermore, the emergence of multidrug-resistant strains threatens to compromise leprosy control (Maeda et al., 2001; Matsuoka et al., 2003). Thus, there is a significant need for new antimycobacterial drugs with novel mechanisms of action.

M. tuberculosis and *M. leprae* produce diesters of long-chain methyl-branched fatty acids (e.g., mycocerosic acids) and long-chain, glycol-containing aliphatic polyketides (e.g., phenolphthiocerols and phthiocerols) that are important small-molecule effectors of virulence (see Onwueme et al. [2005a] for a review). Members of this family of lipid diesters were first established as bona fide virulence factors by Cox et al. (1999) and Camacho et al. (1999). These compounds are noncovalently linked to the outer cell wall layer, and are usually referred to as dimycocerosate esters (DIMs) (Figure 1). DIM variants are produced also by *M. bovis*, *M. kansasii*, *M. marinum*, *M. ulcerans*, *M. microti*, *M. africanum*, *M. haemophilum*, and *M. gastri* (Onwueme et al., 2005a), all of which are pathogenic to humans (Katoch, 2004; Velayati et al., 2005). Production of phenolphthiocerol-based DIM variants (phenolic glycolipids [PGLs]) (Figure 1) has been linked to a hyperlethality phenotype in a mouse model of tuberculosis (Reed et al., 2004) and associated with more severe clinical manifestations in a rabbit model of *M. tuberculosis* meningitis (Tsenova et al., 2005). Conversely, a PGL-deficient *M. bovis* mutant is attenuated in a Guinea pig model of infection (Collins et al., 2005). PGL overproduction by *M. tuberculosis* or addition of purified *M. tuberculosis* PGLs to macrophages reduces proinflammatory cytokine release, whereas loss of PGLs correlates with increased cytokine release by *M. tuberculosis*-infected macrophages (Reed et al., 2004). PGLs of *M. bovis* also reduce proinflammatory cytokine release (Reed et al., 2004). *M. leprae* PGLs induce nerve demyelination, a primary contributing factor to the nerve function impairment characteristic of leprosy (Rambukkana et al., 2002), and are involved in bacterial attachment to and invasion of Schwann cells (Ng et al., 2000). *M. leprae* PGLs also interfere

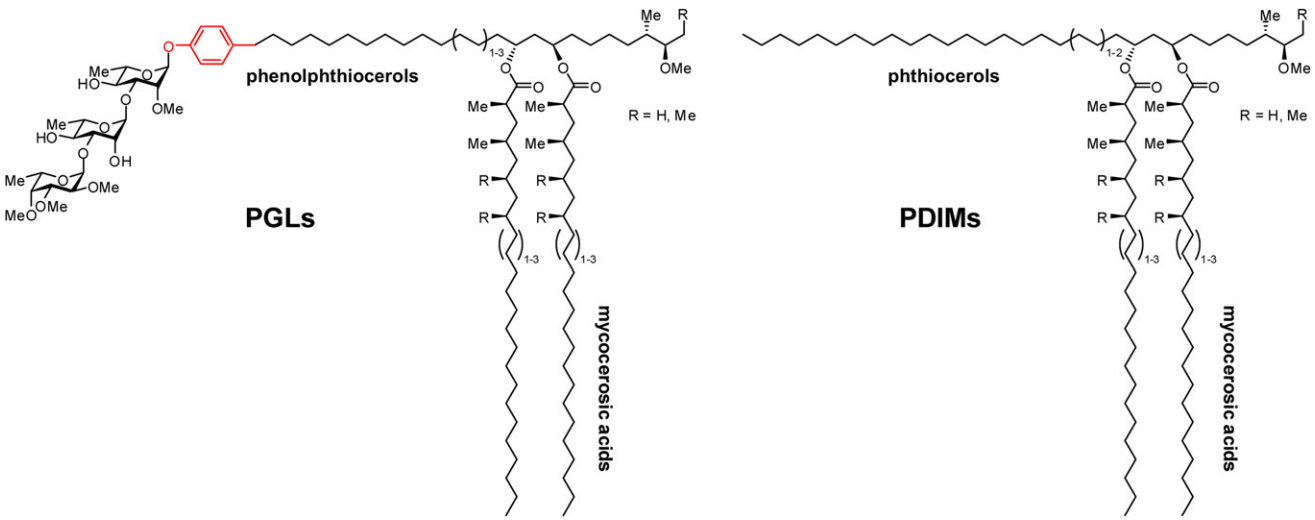

Figure 1. Representative Structures of *M. tuberculosis* Dimycocerosate Esters
The pHBA-derived phenol moiety of the PGLs is highlighted in red.

with antigen-presenting cell function and suppress the proliferative response of T cells to mitogens (Onwueme et al., 2005a). PGLs may also contribute to virulence in other mycobacteria, as evidenced by the recent observation that a DIM-deficient mutant of *M. marinum* is attenuated in a goldfish model of infection (Ruley et al., 2004).

Biosynthesis of the phenolphthiocerol moiety of the PGLs involves the Pks15/1-PpsABCDE type I polyketide synthase system (Azad et al., 1997; Constant et al., 2002; Kolattukudy et al., 1997; Minnikin et al., 2002; Trivedi et al., 2004, 2005), a *trans*-acting enoyl reductase (Simeone et al., 2007a), and two tailoring enzymes that convert phenolphthiodiolones to phenolphthiocerols (Onwueme et al., 2005b; Perez et al., 2004; Simeone et al., 2007b). Feeding experiments with radiolabeled *p*-hydroxybenzoic acid (pHBA) (Daffe and Draper, 1998; Reed et al., 2004) suggest that the *p*-hydroxyphenyl moiety of the PGLs is derived from pHBA, and the *p*-hydroxybenzoyl (pHB) coenzyme A (CoA) thioester has been suggested as the donor of pHBA (Kolattukudy et al., 1997). Despite this progress, the current model for PGL assembly does not contemplate a mechanistic hypothesis for phenolphthiocerol chain initiation. We report herein our investigations of this key step in PGL assembly. Our studies have revealed that a stand-alone, didomain initiation module activates and loads pHBA onto the phenolphthiocerol biosynthesis machinery in a CoA-independent manner. We also report the synthesis and characterization of a small-molecule inhibitor of this module that blocks PGL production.

RESULTS

Bioinformatic-Guided Identification of the Initiation Module of the Phenolphthiocerol Biosynthesis Machinery

We hypothesized that PGL assembly requires formation of a pHB-AMP species that would either undergo transesterification to a pHB-CoA thioester intermediate under the canonical polyketide biosynthesis pathway (Fischbach and Walsh, 2006; Moore and Hertweck, 2002), as suggested previously (Kolattukudy et al., 1997), or, alternatively, acylate an aroyl carrier protein (ArCP) domain thiol directly. The latter case would be in analogy to the biosynthetic pathways of salicylate-derived mycobacterial siderophores (Quadri et al., 1998a) and the 3-amino-5-hydroxybenzoate-derived antibiotic, rifamycin B (Admiraal et al., 2001). We performed protein similarity searches (http://www.ncbi.nlm.nih.gov/blast) with HbaA, a pHB-CoA ligase from *Rhodopseudomonas palustris* (Larimer et al., 2004), as the query to probe the genomes of *M. tuberculosis*, *M. leprae*, and *M. bovis* for possible pHB-AMP and/or pHB-CoA ligases. FadD22 produced the most significant alignment, and is conserved in the three species and annotated as a putative fatty acyl-CoA ligase. Encouragingly, *fadD22* is located between *pks15/1*, proposed to encode a type I polyketide synthase that elongates pHBA to form *p*-hydroxyphenylalkanoate precursors for PGL biosynthesis (Constant et al., 2002), and a chorismate lyase gene, encoding the enzyme that catalyzes the formation of pHBA from chorismate (Stadthagen et al., 2005). FadD22 orthologs are also found in *M. marinum* (Onwueme et al., 2005a) and *M. ulcerans* Agy99 (Stinear et al., 2007). The FadD22 orthologs have 701–708 aa and high sequence identity (73%–100%) (see Figure S1 in the Supplemental Data available with this article online).

Each FadD22 ortholog has an adenylation (AMP-binding, Pfam00501) domain and a 100–150 aa C-terminal extension relative to known acyl-CoA ligases that contains a putative 4′-phosphopantetheine attachment site (Pfam00550; Figure S1), a hallmark of acyl, aroyl, and peptidyl carrier protein domains. This suggested that the adenylation domain forms pHB-AMP and that this intermediate is converted directly to a pHB-*S*-FadD22 thioester by attack of the phosphopantetheine thiol of the ArCP domain (Figure 2A). Thus, we hypothesized that phenolphthiocerol biosynthesis initiation involves FadD22, a stand-alone didomain initiation module that catalyzes formation of a pHB-*S*-ArCP domain thioester *without the intermediacy of pHB-CoA*.

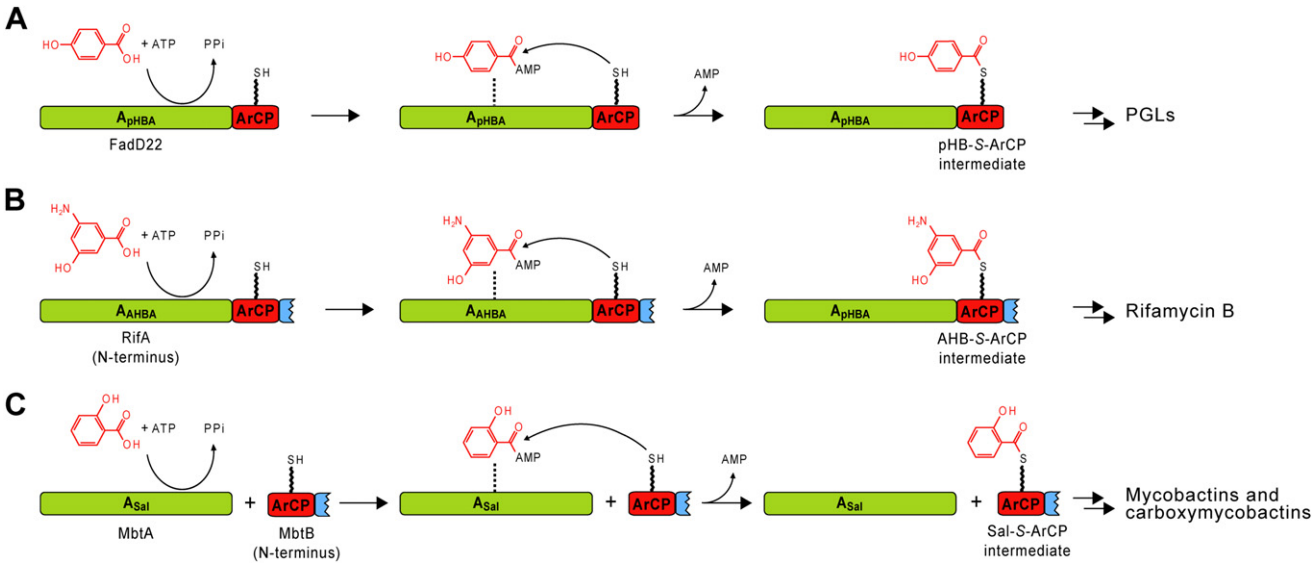

Figure 2. Proposed CoA-Independent Initiation of Phenolphthiocerol Biosynthesis Parallels the Mechanism of Rifamycin B and (Carboxy)-Mycobactin Biosynthesis Initiation

(A) Proposed CoA-independent biosynthesis initiation process required for assembly of the *p*-hydroxyphenyl-polyketide moiety of PGLs.

(B) Mechanism for biosynthesis initiation of rifamycin B.

(C) Mechanism for biosynthesis initiation of mycobactins and carboxymycobactins. A, adenylation domain; ArCP, aroyl carrier protein domain; pHBA, *p*-hydroxybenzoic acid; Sal, salicylic acid; AHBA, 3-amino-5-hydroxybenzoic acid; pHB- /Sal- /AHB-*S*-ArCP, *p*-hydroxybenzoyl- /salicyl- /3-amino-5-hydroxybenzoyl-ArCP domain thioester. Noncovalent binding of acyl-AMP intermediates to the adenylation domains is indicated with a vertical dotted line. The phosphopantetheinyl group in the carrier domains is represented by a wavy line.

fadD22 Is Essential for PGL Production

Based on our bioinformatic analysis, we predicted that FadD22 is essential for PGL biosynthesis. Conversely, this protein would not be required for the biosynthesis of non-pHBA-derived DIM variants based on phthiocerols (PDIMs) and phthiodiolones (PNDIMs) (Figure 1). To investigate these hypotheses, we constructed an *M. bovis* strain with a *fadD22* deletion. To examine the effect of the deletion on DIM production, we used [^{14}C]-pHBA feeding to label PGLs or [^{14}C]-propionate feeding to label both PGLs and PDIMs/PNDIMs (Figure 3A). Analysis of labeled PGLs and PDIMs/PNDIMs from the parental strain and *ΔfadD22* isolates revealed that deletion of *fadD22* abrogates PGL production but not PDIM/PNDIM production (Figure 3B). The *ΔfadD22* strain transformed with pJAM2-FadD22tb (a plasmid expressing *M. tuberculosis fadD22*, identical to *M. bovis fadD22*) produced PGLs, thus ruling out the possibility that the deletion prevents expression of *pks15/1* or other neighboring genes required for PGL production (Figure 3B). Conversely, transformation with the control vector, pJAM2, failed to restore PGL biosynthesis (Figure 3B). In accordance with the fact that PGLs are not required for growth in vitro, no growth difference was observed ex vivo between the parental and mutant strains (Figure S2).

In Vitro Validation of the Catalytic Proficiency of FadD22

To begin assessing the catalytic competence of FadD22, we explored whether nonphosphopantetheinylated (apo) FadD22 (C-terminally hexahistidine-tagged *M. marinum* ortholog; Figure S3) was able to synthesize pHB-AMP. In radiolabeling experiments with both [^{14}C]-pHBA (Figure 4A) and [α-^{32}P]-ATP (data not shown), FadD22 catalyzed the ATP-dependent formation of labeled pHB-AMP as detected by TLC (R_f = ~0.5) and confirmed by LC-MS (Figure 4A; LC-MS analysis not shown; see Experimental Procedures). Based on these analyses, we concluded that FadD22 has pHBA adenylation activity. *M. marinum* FadD22(S576A), a protein variant with the predicted Ser-576 phosphopantetheinylation site substituted by Ala (Figure S3), also catalyzed pHB-AMP formation (Figures 4A–4C), indicating that the conserved Ser is not essential for adenylation activity.

Importantly, addition of CoA to the reactions had no impact on pHB-AMP formation, nor did it result in the formation of additional radiolabeled products detectable by TLC. In particular, pHB-CoA formation was not detected by TLC (Figure 4B) or LC-MS (data not shown). In contrast, pHB-CoA (R_f = 0.37) formation was detected in controls with a *R. palustris* benzoyl-CoA ligase (Beuerle and Pichersky, 2002) that accepts pHBA as a substrate (Figure 4B and LC-MS analysis not shown; see Experimental Procedures). As expected, benzoyl-CoA ligase-dependent accumulation of the pHB-AMP intermediate was observed in absence of CoA (Figure 4B). Overall, these observations support the view that FadD22 is not a pHB-CoA ligase.

Time courses of pHB-AMP formation by apo-FadD22 and FadD22(S576A) revealed a maximum pHB-AMP accumulation corresponding to a pHB-AMP:enzyme ratio of ~5, suggesting only five catalytic turnovers and that adenylation is inhibited by the acyl-AMP intermediate (Figure 4C). However, the binding of the intermediate to the enzyme does not appear to be tight enough to stop adenylate accumulation at 1:1 stoichiometry. Overall, this is consistent with the fact that mechanistically related acyl adenylate-forming enzymes bind (noncovalently) their cognate acyl-AMP intermediates 2–3 orders of magnitude more

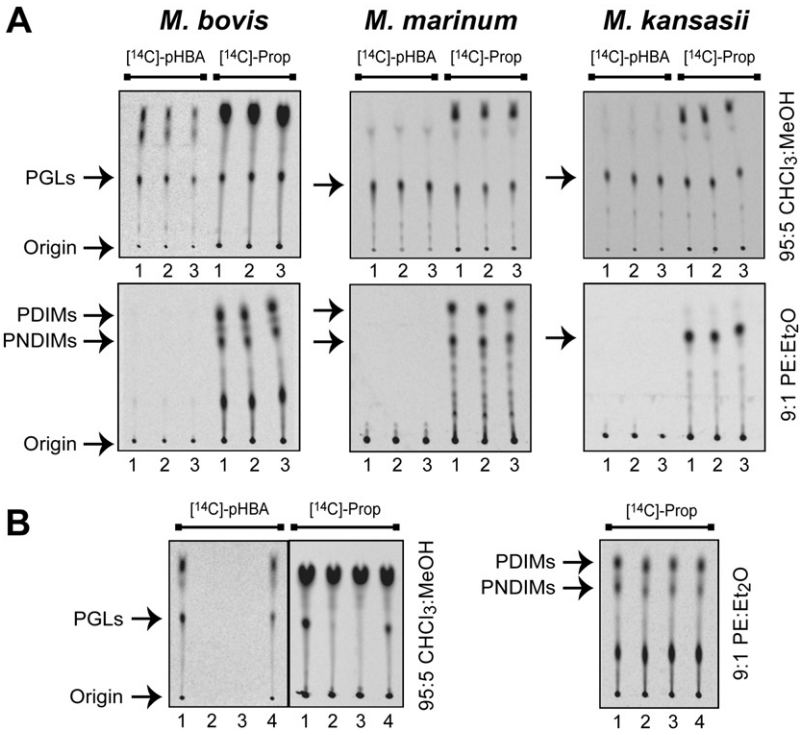

Figure 3. FadD22 Is Required for PGL Production but Not for PDIM or PNDIM Production

(A) TLC analysis of DIMs from *M. bovis*, *M. marinum*, and *M. kansasii* showing incorporation of the label of [^{14}C]-*p*-hydroxybenzoic acid (pHBA) in PGLs and [^{14}C]-propionate (Prop) in PGLs, PDIMs, and PNDIMs. The profile of triplicate labeling experiments (lanes 1, 2, and 3) are shown in each panel. *M. kansasii* lacks PDIMs due to a (phenol)phthiodiolone ketoreductase deficiency.

(B) Radio-TLC analysis demonstrating that *fadD22* is required for PGL production, but not for PDIM/PNDIM production. [^{14}C]-labeled apolar lipids of *M. bovis* strains wild-type (lane 1), *ΔfadD22* (lane 2), *ΔfadD22* with vector pJAM2 (lane 3), and *ΔfadD22* with pJAM2-*fadD22tb* (pJAM2 expressing FadD22) (lane 4). Indicated TLC eluents were used for PGL and PDIM/PNDIM visualization as reported (see Experimental Procedures). PE, petroleum ether; Et_2O, diethyl ether. PGLs remain at the origin with PE/Et_2O (9:1, v/v) eluent. PDIMs/PNDIMs run with the eluent front in $CHCl_3$/MeOH (95:5, v/v).

tightly than their carboxylic acid and ATP substrates (Kim et al., 2003; May et al., 2002; Norris and Berg, 1964; Webster, 1963). It is likely that pHB-AMP is sequestered in the adenylation domain until transesterification to the ArCP domain liberates the adenylation domain for another catalytic cycle.

To investigate whether apo-FadD22 retains bound pHB-AMP, we examined the enzyme and [^{14}C]-pHB-AMP elution patterns obtained when [^{14}C]-pHB-AMP formation reactions were subjected to size-exclusion chromatography. pHB-AMP coeluted with the enzyme, rather than following the small-molecule elution profile delineated by [^{14}C]-pHBA (Figure 4D). Equivalent results were obtained with FadD22(S576A) (data not shown). We verified that the acyl adenylate intermediate is stable in solution for at least 2 hr at 37°C (Figure S4), thus excluding the possibility that the lack

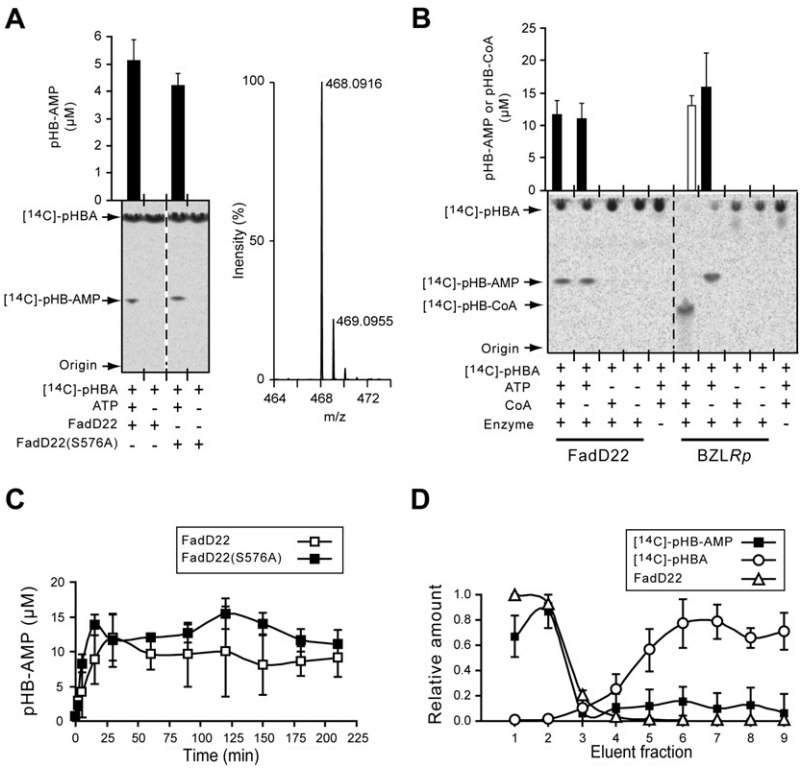

Figure 4. Formation of pHB-AMP by FadD22 and FadD22(S576A)

(A) TLC analysis of radiolabeled pHB-AMP formation. Enzymes were included at 5 μM in the reactions. No product was detected in reaction without enzyme (data not shown). The mass spectrum of the pHB-AMP product is shown.

(B) Influence of CoA on pHB-AMP formation. Substrates and enzymes (5 μM) included in the reactions are indicated. BZLR*p*, *R. palustris* benzoyl-CoA ligase.

(C) Time course for pHB-AMP formation by FadD22 (2 μM) and FadD22(S576A) (2 μM).

(D) FadD22-pHB-AMP association determined by size exclusion chromatography. FadD22 was included at 15 μM in the reaction. Graphs show means of triplicate reactions with SEM. Only one of the triplicate reactions is shown in the representative TLC image below each graph in (A) and (B). pHB-AMP, black bars; pHB-CoA, white bars.

of a significant amount of free, unbound intermediate is due to rapid hydrolysis of released pHB-AMP. Reasonable stability of pHB-AMP and comparable intermediates in aqueous solutions has been reported (Niu et al., 2006). Thus, the elution pattern of pHB-AMP is in agreement with the formation of a stable, noncovalent FadD22•pHB-AMP complex.

The second step in our proposed initiation mechanism is transesterification of the *p*-hydroxybenzoyl moiety from pHB-AMP to the phosphopantetheinylated (holo) ArCP domain (Figure 2A). We developed a phosphopantetheinylation assay based on FlashPlate technology (Brown et al., 1997) (see Supplemental Experimental Procedures) to investigate whether FadD22 and FadD22(S576A) are targets for phosphopantetheinylation. In this assay, we used the phosphopantetheinyl transferase, Sfp (Quadri et al., 1998b), and probed for incorporation of [^{3}H]-phosphopantetheinyl group into these proteins. These studies demonstrated that apo-FadD22 is a substrate for phosphopantetheinylation, while FadD22(S576A) is not (Figure 5A). These results support the presence of a carrier protein domain in FadD22 and the role of Ser-576 as the modification site. We also found that FadD22, coexpressed with Sfp (to obtain holo-FadD22), could not be [^{3}H]-phosphopantetheinylated in vitro (data not shown), suggesting that Sfp-dependent phosphopantetheinylation of FadD22 in *Escherichia coli* proceeds with ~100% efficiency.

The ability to obtain holo-FadD22 enabled us to explore whether FadD22 is competent for pHB-*S*-FadD22 formation (Figure 2A). This autoacylation was assayed by probing for covalent incorporation of a [^{14}C]-pHBA-derived label into purified holo-FadD22. We also examined [^{14}C]-pHBA loading onto apo-FadD22 and FadD22(S576A). Holo-FadD22 was readily autoacylated in an ATP-dependent and CoA-independent manner (Figure 5B). Maximum autoacylation reached 100% (Figure 5D), in agreement with the 100% conversion of apo- to holo-protein inferred from the phosphopantetheinylation analysis. Conversely, neither apo-FadD22 nor FadD22(S576A) were capable of autoacylation (Figure 5B). These observations indicate that FadD22 is not phosphopantetheinylated to a meaningful degree in *E. coli* in the absence of Sfp. Apo-FadD22 and FadD22(S576A), like holo-FadD22, are able to form pHB-AMP (Figure 5C), and we attribute their lack of starter unit loading to the absence of the phosphopantetheine prosthetic group. Overall, our studies of FadD22 demonstrate its pHBA adenylation activity, its apo- to holo-protein conversion by phosphopantetheinylation, and its self-loading with pHBA.

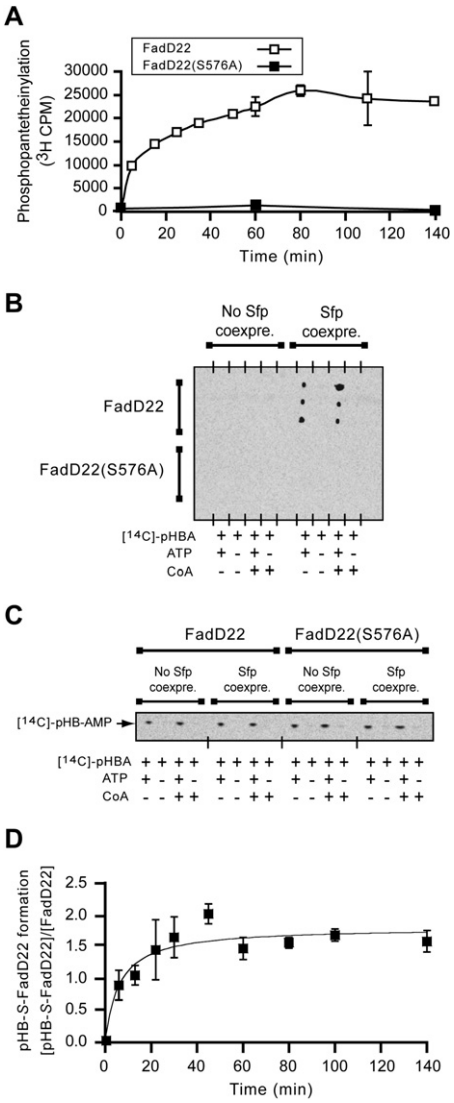

Figure 5. FadD22 Is Phosphopantetheinylated and Autoacylated with the pHBA, whereas FadD22(S576A) Is Not

(A) Time course for in vitro phosphopantetheinylation of wild-type FadD22 (1 μM) and FadD22(S576A) (1 μM).

(B) Autoloading competence of FadD22 and FadD22(S576A) expressed alone or together with Sfp. Proteins (10 μM) in acylation reactions with the indicated compositions were bound to the membrane under denaturing conditions for analysis of covalently bound radiolabel in the proteins. Only holo-FadD22 was competent for autoacylation (upper right quadrant). Triplicate reactions were spotted on the membrane.

(C) pHB-AMP formation competence of FadD22 (10 μM) and FadD22(S576A) (10 μM) expressed alone or together with Sfp. TLC excerpt image shows formed pHB-AMP (or lack thereof) in reactions of the indicated composition.

(D) Time course for holo FadD22 autoacylation. The concentration of the pHB-*S*-FadD22 formed was normalized to the concentration of FadD22 (5 μM) in the reaction ([pHB-*S*-FadD22]/[FadD22]). Means of triplicate reactions with SEM are shown.

Design, Synthesis, and Biological Evaluation of a PGL Biosynthesis Inhibitor

We and others have recently described a nonhydrolyzable mimic of salicyl-AMP, salicyl-AMS (5′-*O*-[*N*-salicylsulfamoyl]-adenosine), as a tight-binding inhibitor of salicylic acid adenylation domains (Ferreras et al., 2005; Miethke et al., 2006; Somu et al., 2006). Based on this precedent, we postulated that nonhydrolyzable pHB-AMP analogs would inhibit the adenylation domain of FadD22. To evaluate this idea, we synthesized the pHB-AMP analog 5′-*O*-[*N*-(4-hydroxybenzoyl)sulfamoyl]-adenosine (**2**) (pHB-AMS) (Figure 6A and Figure S5), and tested the activity of this compound in pHB-AMP and pHB-*S*-FadD22 formation assays and DIM production assays. pHB-AMS inhibited both pHB-AMP formation (IC_{50} = 6 μM; Figure 6B) and pHB-*S*-FadD22 formation (IC_{50} = 11 μM; Figure 6C) with IC_{50} values that are less than 10 times the enzyme concentration, a characteristic of tight-binding inhibitors (Copeland, 2000). When tested in PGL and PDIM/PNDIM production assays with

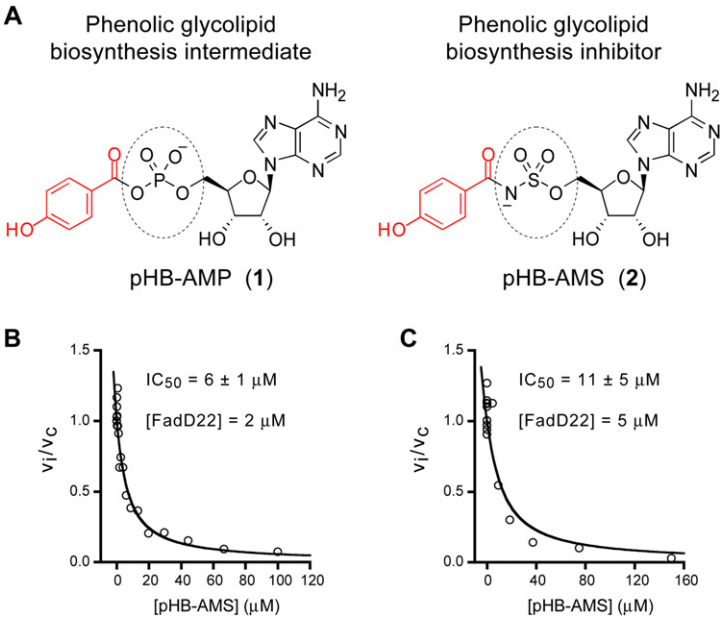

Figure 6. pHB-AMS Inhibits FadD22-Catalyzed pHBA Adenylation and Autoacylation

(A) *p*-Hydroxybenzoyl-AMP (**1**) (pHB-AMP) intermediate and its mimic, 5′-*O*-(*N*-[4-hydroxybenzoyl]sulfamoyl)adenosine (**2**) (pHB-AMS).

(B) Dose-response for inhibition of pHB-AMP formation plotted with fractional velocity as a function of pHB-AMS concentration.

(C) Dose-response for inhibition of pHB-*S*-FadD22 formation plotted with fractional velocity as a function of pHB-AMS concentration. v_i and v_c, are velocities in inhibitor- and DMSO-containing reactions, respectively. Data points are means of triplicate reactions.

M. tuberculosis, *M. marinum*, *M. kansasii*, and *M. bovis* (data not shown), pHB-AMS strongly inhibited PGL production in all four species at up to 14- to 48-fold reduction (Figure 7A). Interestingly, this dramatic inhibition of PGL production correlated with a slight (1.3- to 3.4-fold) increase in PDIM/PNDIM production (Figure 7A), probably due to augmented availability of enzymes and building blocks for PDIM/PNDIM assembly arising from metabolic flux redirectioning upon PGL biosynthesis shutdown. We also demonstrated that increasing the intracellular concentration of FadD22 or its adenylation domain reduced the effectiveness of pHB-AMS (Figure 7B). This result is in line with an expected inhibitor titration effect and provides additional evidence that the adenylation domain of FadD22 is the cellular target of pHB-AMS in the PGL pathway.

Since PGLs are dispensable for ex vivo growth, pHB-AMS is not expected to have antimicrobial activity in vitro. Thus, to assess the selectivity of this compound, we examined its activity against *M. tuberculosis*, *M. bovis*, *M. marinum*, and *M. kansasii*. As expected, pHB-AMS ($\leq$800 μM) had no effect on growth in cultures started with the high inoculum used in the PGL inhibition experiments described above ($OD_{580\ nm}$ = 0.6). Very modest growth inhibition was detected at the maximum compound concentration in *M. tuberculosis* and *M. bovis* cultures started with low inoculum ($OD_{580\ nm}$ = 0.001), which affords a more sensitive setting for antimicrobial activity detection. This suggests that the inhibitor has only a marginal off-target effect, which is detectable at a considerably high compound-to-cell ratio. These results provide important support for the selectivity of pHB-AMS in targeting mycobacterial PGL biosynthesis.

DISCUSSION

Several mycobacterial pathogens produce PGLs, a family of surface-exposed bioactive glycolipids that function as small-molecule effectors in the host-pathogen interplay and contribute to virulence. The work presented here provides the first insights into the molecular mechanism of phenolphthiocerol biosynthesis initiation, a fundamental step in PGL assembly. Our studies led to the identification of FadD22 as a stand-alone, didomain loading module that is integral to the phenolphthiocerol biosynthesis machinery. FadD22 is responsible for CoA-independent activation and charging of a pHBA starter unit to form pHB-*S*-FadD22, the first committed acyl-*S*-enzyme covalent intermediate in the phenolphthiocerol chain assembly line.

Our in silico analysis pointed to the orphan protein, FadD22, previously annotated as a putative fatty acyl-CoA ligase, as the lead candidate for the initiation module required for phenolphthiocerol biosynthesis. Our genetic analysis has shown that *fadD22* is essential for PGL production and our in vitro analysis of FadD22 has validated the functionality of its adenylation and ArCP domains. The catalytic partnership of these two domains leads to formation of pHB-*S*-FadD22. We propose that this charged module primes phenolphthiocerol biosynthesis by presenting the starter unit for the first extension cycle of the *p*-hydroxyphenyl-polyketide formation process. Starter unit extension is then carried out by the next enzyme in the phenolphthiocerol assembly line—probably Pks15/1. Our ability to obtain pHB-*S*-FadD22 will facilitate future enzymological studies to decipher the functional cooperation of this initiation module with Pks15/1 or other potential enzyme partners in the phenolphthiocerol assembly line.

The CoA independence of the phenolphthiocerol biosynthesis initiation mechanism parallels that observed in the biosynthetic pathway of rifamycin B (Admiraal et al., 2001). The rifamycin B system initiation module consists of an adenylation domain for 3-amino-5-hydroxybenzoate and its partner ArCP domain for formation of a 3-amino-5-hydroxybenzoyl-*S*-ArCP domain intermediate (Figure 2B). The mechanism of phenolphthiocerol biosynthesis initiation is also reminiscent of that observed in the biosynthesis of the salicylate-capped, hybrid, nonribosomal peptide-polyketide (carboxy)mycobactin siderophores produced by *M. tuberculosis* and other *Mycobacterium* spp. (Quadri et al., 1998a). During the biosynthesis of these siderophores, MbtA catalyzes adenylation of salicylic acid and subsequent transesterification onto a holo-ArCP domain located at the N terminus of the nonribosomal peptide synthetase MbtB (Figure 2C). The parallel, aryl acid-specific, adenylation-ArCP didomain composition of the initiation machinery of the phenolphthiocerol and siderophore pathways suggests an intriguing possible evolutionary relationship between the PGL and the siderophore

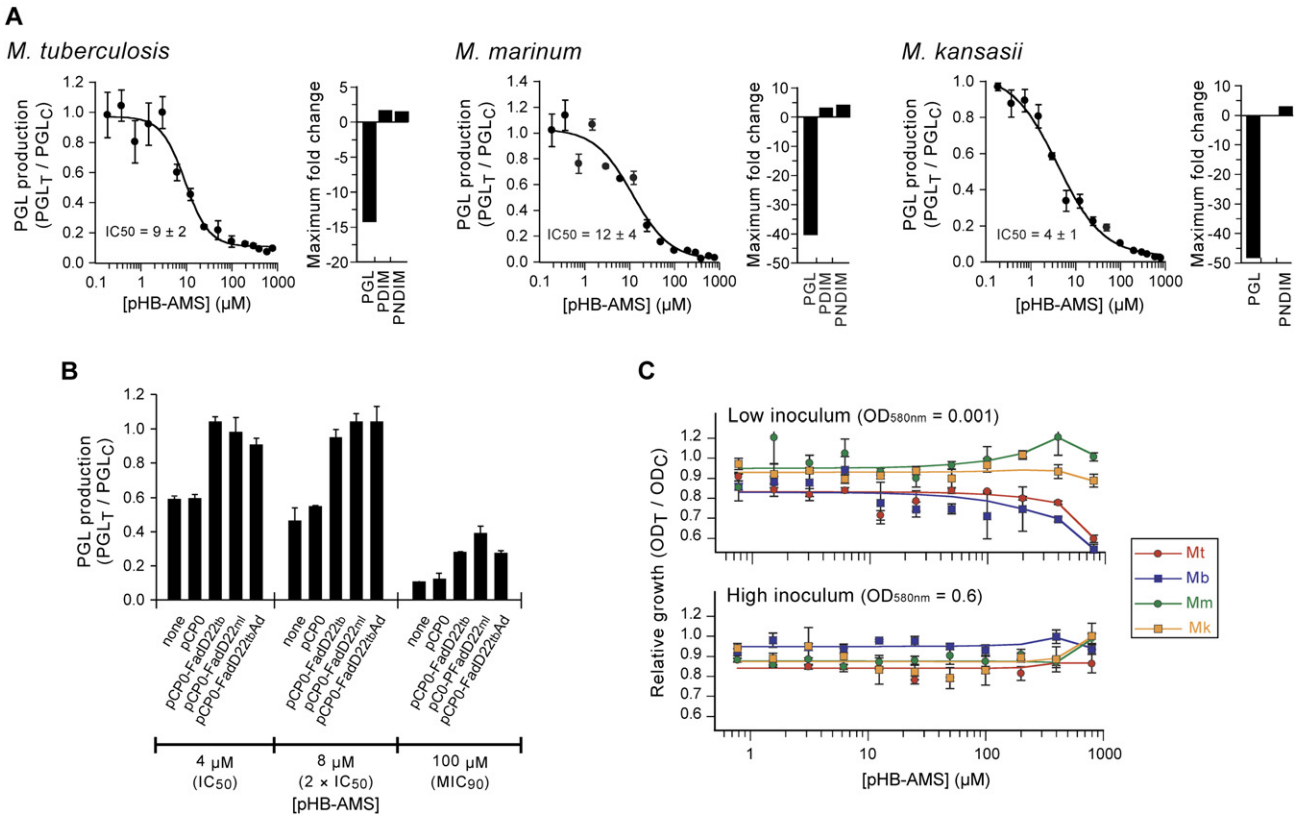

Figure 7. pHB-AMS Inhibits PGL Production

(A) Inhibition of PGL production by pHB-AMS. The dose-response plots show the effect of pHB-AMS on production of PGLs. PGL_T/PGL_C, ratio of PGL production in inhibitor-treated (PGL_T) to DMSO-treated (PGL_C) cultures. Values represent means from triplicate cultures (±SEM). The maximum fold changes induced by pHB-AMS on PGL, PDIM, and PNDIM production are depicted in the bar graphs. No PDIM fold change is shown for *M. kansasii*, which is PDIM deficient.

(B) Reduction of the PGL production inhibitory efficacy of pHB-AMS by multicopy suppressor effect. pHB-AMS was tested at the concentration shown against *M. kansasii* (Mk) and Mk transformed with the indicated plasmids. pCP0, vector; pCP0-FadD22tb, pCP0 expressing *M. tuberculosis* FadD22; pCP0-FadD22tbAd, pCP0 expressing *M. tuberculosis* FadD22 adenylation domain; pCP0-FadD22ml, pCP0 expressing *M. leprae* FadD22. Data represent means of triplicate cultures (±SEM).

(C) Effect of pHB-AMS on growth of *M. tuberculosis* (Mt, red circles), *M. bovis* (Mb, blue squares), *M. marinum* (Mm, green circles), and *M. kansasii* (Mk, orange squares). The effect was evaluated on cultures started with the indicated inoculum levels. OD_T/OD_C, ratio of $OD_{580\ nm}$ of inhibitor-treated (OD_T) to $OD_{580\ nm}$ of DMSO-treated (OD_C) cultures. Means of triplicate cultures (±SEM) are shown.

biosynthesis machinery. Interestingly, the adenylation-ArCP didomain architecture differs between these three aryl acid-specific loading systems. While FadD22 is a stand-alone didomain module, the rifamycin B system has a didomain initiation module that is part of a larger protein (RifA) containing three polyketide synthase modules, while the siderophore pathway features an in *trans* loading strategy with a stand-alone adenylation domain and an ArCP domain fused to an additional module in MbtB (Figure 2).

The mechanistic insights into phenolphthiocerol biosynthesis initiation provided us with a framework to design a small-molecule inhibitor of PGL biosynthesis, pHB-AMS. The inhibitory activity of pHB-AMS in enzymatic and cellular assays affords additional support for our model of phenolphthiocerol biosynthesis initiation. These studies also provide proof-of-principle for the drugability of the PGL pathway and for inhibition of the biosynthesis of a bona fide polyketide virulence factor. It has been suggested that drugs that inhibit the biosynthesis or the function of virulence factors may be combined with classical antimicrobials to afford more efficient treatments against infections (Alksne and Projan, 2000; Clatworthy et al., 2007; Marra, 2004; Quadri, 2007). It is interesting to speculate that drugs that block PGL biosynthesis may reduce the adaptive fitness of PGL-producing *M. tuberculosis* strains in the human host by eliminating PGL-dependent immunomodulatory effects. These drugs may also diminish the ability of *M. leprae* to invade Schwann cells and cause nerve function impairment. Thus, pHB-AMS represents an initial lead compound for exploring the potential therapeutic value of PGL biosynthesis inhibitors in animal infection models in the future.

SIGNIFICANCE

Mycobacterial PGLs are a family of surface-exposed bioactive glycolipids that function as small-molecule effectors in the host-pathogen interplay and contribute to virulence. Understanding the biosynthesis of these and other effectors of mycobacterial virulence is an important goal, as it may lead to new therapeutics. The studies reported here illuminate

the mechanism of chain initiation required for the assembly of the phenolphthiocerol moiety of PGLs. Our results support a model in which a stand-alone, didomain initiation module comprised of a pHBA adenylation domain and an aroyl carrier protein domain forms an acyl-*S*-enzyme covalent intermediate in the *p*-hydroxyphenyl-polyketide chain assembly line. The stand-alone status of this initiation module sets it apart from related aryl acid primer unit didomain loading systems characterized previously. Moreover, to our knowledge, FadD22 is the first characterized, bona fide pHBA-specific initiation module implicated in a polyketide biosynthetic pathway. Lastly, the insights gained on the mechanism of phenolphthiocerol biosynthesis initiation allowed us to develop an inhibitor of PGL assembly with potent activity in several mycobacterial pathogens. Overall, these studies advance our understanding of the biosynthesis of an important group of small-molecule effectors of mycobacterial virulence and provide important support for the feasibility of targeting PGL biosynthesis to develop new drugs to treat mycobacterial infections.

EXPERIMENTAL PROCEDURES

Mycobacterial Strains and Growth Conditions

Mycobacteria were grown in Middlebrook 7H9 (Difco) supplemented with 10% albumin dextrose complex (Difco) and 0.1% Tween-80 or Middlebrook 7H11 plates (Difco) containing 10% oleic acid albumin dextrose complex (Difco). *M. tuberculosis* Canetti, *M. bovis* BCG, and *M. kansasii* were cultured at 37°C. *M. marinum* was cultured at 28°C. When required, kanamycin (30 μg/ml), hygromycin (50 μg/ml) and/or sucrose (2%) were added to the media.

DIM Production Analysis

Cultures grown for 8 d (*M. tuberculosis* and *M. bovis*) or 7 d (other species) were diluted in fresh medium to an $OD_{580\ nm}$ of 0.6 and loaded into 12 well plates (1 ml/well). Wells were treated (in triplicate) with 0.8% DMSO (controls) or pHB-AMS at different concentrations, and 0.8% DMSO. [1-C^{14}]-propionate (specific activity = 54 mCi/mmol; ARC, Inc.) was added to each well at 0.2 μCi/ml and plates were incubated for 12 hr before the OD of the cultures was measured and cells were harvested for apolar lipid extraction. Apolar lipids were extracted with a biphasic mixture of methanolic saline and petroleum ether (PE) as previously described (Onwueme et al., 2004, 2005b). PGLs in apolar lipid extracts were analyzed by TLC on aluminum-backed 250 μm silica gel plates (EM Science) with $CHCl_3$/MeOH (95:5, v/v) eluent as previously reported (Constant et al., 2002; Papa et al., 1987; Perez et al., 2004). PDIMs and PNDIMs were analyzed by TLC with PE/diethyl ether (Et_2O) (9:1, v/v) eluent as previously reported (Onwueme et al., 2004; Onwueme et al., 2005b). Plates were exposed to phosphor screens, which were scanned with a Typhoon Trio Imager (Amersham Biosciences). PGL, PDIM, and PNDIM signals were quantified with ImageQuant v1.2 (Molecular Dynamics). Dose-response graphs for these and other experiments presented here were generated with KaleidoGraph 4.0. IC_{50} values were calculated by fitting the data to the sigmoid equation:

$$\frac{S_i}{S_c} = b + \frac{(a-b)}{1+([I]/IC_{50})^s}, \quad (1)$$

where: S_i and S_c are the background-corrected signals of the lipids in the inhibitor-treated cultures and DMSO controls respectively; a and b are the top and bottom of the curve, respectively; and s is the Hill coefficient.

Growth Inhibition Assay

Cultures grown for 7 d were diluted in Middlebrook 7H9 to an $OD_{580\ nm}$ of 0.6 or 0.001 and loaded in 96 well plates (200 μl/well). Wells were treated (in triplicate) with 0.8% DMSO (controls) or pHB-AMS at different concentrations, and 0.8% DMSO. Plates were incubated for growth for 10 d and $OD_{580\ nm}$ was monitored daily in a Spectra Max Plus reader (Molecular Dynamics).

Construction of a *ΔfadD22* Mutant

The *ΔfadD22* mutant was engineered by the p2NIL/pGOAL method as previously reported (Parish and Stoker, 2000) (Supplemental Experimental Procedures). Briefly, we constructed a *ΔfadD22* cassette-delivery suicide vector carrying a deletion cassette that contains a 5′ arm (1.2 kb region upstream of *fadD22* and *fadD22*'s start codon) and a 3′ arm (*fadD22*'s last 10 codons and the downstream 810 bp segment) (Figure S2). The C-terminal codons were preserved due to sequence overlap with *pks15/1*. This vector was introduced into *M. bovis* and mutants with *fadD22* replaced by the *ΔfadD22* cassette via double-crossover were selected and identified by previously reported methods (Onwueme et al., 2004; Parish and Stoker, 2000).

Plasmids for Protein Expression in Mycobacteria

pJAM-FadD22tb, pJAM-FadD22tbAd, and pJAM-FadD22ml were based on the mycobacterial expression vector pJAM2 (Triccas et al., 1998) and express the mycobacterial genes under control of the acetamidase promoter. pCP0-FadD22tb, pCP0-FadD22tbAd, and pCP0-FadD22ml were based on the mycobacterial expression vector, pCP0, and express the mycobacterial genes under control of the *hsp60* promoter (Onwueme et al., 2004). See the Supplemental Experimental Procedures for plasmid construction.

pHB-AMP and pHB-CoA Formation

Reaction contained 75 mM MES [pH 6.5], 0.5 mM $MgCl_2$, 1 mM TCEP, 50 μM [^{14}C]-pHBA, and, depending on the specific reaction indicated, combinations of the following components: 1 mM ATP, 100 μM CoA, 0.5 μM Sfp, 5 μM FadD22, 5 μM FadD22(S576A), or 5 μM BZL*Rp*. Reactions were incubated for 2 hr at 30°C and product formation was analyzed by radiometric TLC with Al Sil G/UV TLC plates (Whatman) and ethyl acetate (EtOAc)/isopropyl alcohol/acetic acid/water (70:20:25:40, v/v) eluent. Plates were exposed to phosphor screens. The screens were scanned with a Typhoon Trio Imager and signal intensity was quantified with ImageQuant v1.2 software. For time-course experiments, pHB-AMP formation reactions (100 μl) containing 75 mM MES [pH 6.5], 0.5 mM $MgCl_2$, 1 mM TCEP, 1 mM ATP, 50 μM [^{14}C]-pHBA, and 2 μM of either FadD22 or FadD22(S576A) were incubated at 30°C. Reaction samples were taken at different times for TLC analysis and pHB-AMP quantification. Concentrations of [^{14}C]-pHB-AMP (or [^{14}C]-pHB-CoA) were calculated with calibration curves obtained by linear regression fitting to calibration data generated by spotting known amounts of [^{14}C]-pHBA on the plates after chromatography. The identity of pHB-AMP and pHB-CoA products was confirmed by LC-MS analysis of the (unlabeled) compounds isolated by preparative TLC. pHB-CoA: $[M+H]^+$ *m/z* observed, 888.1432, calculated, 888.1436; $[M-H]^-$ *m/z* observed, 886.1288, calculated, 886.1280; (data not shown). pHB-AMP: $[M+H]^+$ *m/z* observed, 468.0916 (Figure 4A), calculated, 468.0915; $[M-H]^-$ *m/z* observed, 466.0769 (data not shown), calculated, 466.0769. The proteins used in these and other experiments here were expressed in *E. coli* and purified as described in the Supplemental Experimental Procedures.

LC-MS Analysis

pHB-AMP and pHB-CoA were purified from pHB-AMP and pHB-CoA formation reactions, respectively, by preparative TLC. The product was eluted with methanol, and the extract was subjected to LC-MS analysis. Other samples for LC-MS analysis were prepared as follows: reactions (100 μl) containing 5 mM MES [pH 6.5], 0.5 mM $MgCl_2$, 1 mM TCEP, and, depending on the reaction, 1 mM ATP, 1 mM pHBA, 1 mM CoA, and 10 μM of either FadD22 or BZL*Rp*, were incubated 2 hr at 30°C in Mini Dialysis Units (Slide-A-Lyzer; cutoff: 3.5 kDa; Pierce). Each unit was kept in contact with 100 μl of a reaction mixture lacking enzyme so that released products accumulated in the enzyme-free mixture, which was then subjected to LC-MS analysis. Samples were analyzed on an Agilent Technologies 6210 high-resolution time-of-flight MS connected to an Agilent Technologies 1200 capillary HPLC system. See the Supplemental Experimental Procedures for details.

FadD22-pHB-AMP Complex Formation

pHB-AMP formation reactions containing 75 mM MES [pH 6.5], 0.5 mM $MgCl_2$, 1 mM TCEP, 1 mM ATP, [^{14}C]-pHBA, and 15 μM FadD22 were incubated for

10 min at 30°C. After incubation, 50 μl reaction aliquots were applied to Gel Filtration G-50 Macrospin Columns (The Nest Group, Inc.) equilibrated with 75 mM MES [pH 6.5]. Columns were centrifuged (3 min, 110 × g) and flowthrough fractions were collected. The columns were then successively washed with aliquots of 75 mM MES [pH 6.5] (50 μl) and the flowthrough fractions were collected. For each flowthrough fraction, a sample (5 μl) was subjected to TLC analysis and pHB-AMP quantification, and a 10 μl sample was analyzed by SDS-PAGE (12.5%). Gels were stained with GelCode Blue stain (Pierce) and photographed. Densitometric analysis to quantify protein bands was performed with Quantity One 4.5.2 software (Bio-Rad Laboratories).

In Vitro Phosphopantetheinylation

Reactions (50 μl) containing 75 mM Tris·HCl [pH 7.5], 10 mM $MgCl_2$, 1 mM TCEP, 1 μM CoA (4′-phosphopanetheine-^{3}H; 11 Ci/mmol; ARC, Inc.), 0.25 μM Sfp (absent in negative controls), and 0.75 μM of either FadD22, FadD22(S576A), FadD22 coexpressed with Sfp, or FadD22(S576A) coexpressed with Sfp were incubated for 1 hr at 37°C. After incubation, reactions were diluted with 150 μl of PBS containing 20% MeOH, 1 mM CoA, and 0.1% BSA, and the mixtures were transferred to 96 well Ni^{2+}-chelate-coated FlashPlate Plus plates (Perkin Elmer). After tagged protein binding (overnight at 4°C), wells were washed with PBS (3 × 300 μl) and well-bound counts were quantified in a Wallac Microbeta counter. Counts were converted to amounts of phosphopantetheinylated protein with the specific activity of [^{3}H]-CoA. For time-dependent phosphopantetheinylation experiments, reactions (50 μl) containing 75 mM Tris·HCl [pH 7.5], 10 mM $MgCl_2$, 1 mM TCEP, 0.3 μM [^{3}H]-CoA, 0.25 μM Sfp, and 1 μM of either FadD22 or FadD22(S576A) were diluted as described above at different times and transferred to the plates for protein binding and phosphopantetheinylation quantification.

In Vitro pHB-Protein Thioester Formation

Reactions (60 μl) containing 75 mM MES [pH 6.5], 0.5 mM $MgCl_2$, 1 mM TCEP, 50 μM [^{14}C]-pHBA, and, depending on the reaction indicated, 1 mM ATP, 100 μM CoA, and 10 μM of either FadD22, FadD22(S576A), FadD22 coexpressed with Sfp, or FadD22(S576A) coexpressed with Sfp were incubated for 1 hr at 30°C. After incubation, reaction aliquots (10 μl) were diluted with PBS (15 μl) containing 2.5 mM pHBA and 20% MeOH. The mixtures were transferred to nitrocellulose membranes (pore size, 0.2 μm, Protran; Whatman) for protein binding with Minifold I Slot Blot System (Whatman). Membranes were washed sequentially with PBS containing 20% MeOH (3 × 25 ml) and 10% TCA (25 ml), and then exposed to phosphor screens. Phosphor screens were scanned and signal intensity was quantified as described previously here. Amounts of [^{14}C]-pHB-protein thioester in the samples were calculated with calibration curves obtained by linear regression fitting to calibration data generated from known amounts of [^{14}C]-pHBA spotted on the membranes. An additional 4 μl aliquot was taken from each reaction and subjected to TLC and pHB-AMP quantification as described previously here. For time-course experiments, aliquots from pHB-protein thioester formation reactions (75 mM MES [pH 6.5], 0.5 mM $MgCl_2$, 1 mM TCEP, 1 mM ATP, 50 μM [^{14}C]-pHBA, and 5 μM FadD22 coexpressed with Sfp) taken at different times were diluted and analyzed for [^{14}C]-pHB-protein thioester formation, as described previously here.

Inhibition of pHBA Adenylation

Reactions (20 μl) containing 75 mM MES [pH 6.5], 0.5 mM $MgCl_2$, 1 mM TCEP, 1 mM ATP, 50 μM [^{14}C]-pHBA, 2 μM FadD22, and 0.15% DMSO (controls) or 0.15% DMSO and pHB-AMS at different concentrations were incubated for 1 hr at 30°C. After incubation, reaction aliquots were subjected to TLC analysis and pHB-AMP quantification, as noted previously here. Sets of dose-response data were fitted to the Morrison equation for tight-binding inhibitors

$$\frac{v_i}{v_c} = 1 - \frac{([E] + [I] + K_i^{app}) - \sqrt{([E] + [I] + K_i^{app})^2 - 4[E][I]}}{2[E]}, \quad (2)$$

where E = enzyme; I = inhibitor; and v_i and v_c = velocities in the presence and absence of inhibitor, respectively (Copeland, 2000). IC_{50} values were calculated with the equation for tight-binding inhibitors

$$IC_{50} = \frac{1}{2}[E] + K_i^{app}, \quad (3)$$

with K_i^{app} values derived from the curve fit (Copeland, 2000). The inhibitor used in these and other studies described here was synthesized by 5′-*O*-sulfamoylation of a protected adenosine derivative, followed by *N*-acylation of the sulfamate with *p*-acetoxybenzoic acid and removal of protecting groups (see Supplemental Experimental Procedures and Figure S5).

Inhibition of pHB-Protein Thioester Formation

pHB-protein thioester formation reactions (20 μl) containing 75 mM MES [pH 6.5], 0.5 mM $MgCl_2$, 1 mM TCEP, 1 mM ATP, 50 μM [^{14}C]-pHBA, 5 μM FadD22 coexpressed with Sfp, and 0.15% DMSO (controls) or 0.15% DMSO and pHB-AMS at different concentrations were routinely incubated for 40 min at 30°C. After incubation, 40 μl of PBS containing 20% MeOH and 1 mM pHBA were added to each reaction, and 30 μl of each mixture was transferred to nitrocellulose membranes for quantification of [^{14}C]-pHB-protein thioester in the samples, as noted previously here. Sets of dose-response data were fitted to Equation 2 and IC_{50} values were calculated with Equation 3, as described previously here.

Supplemental Data

Supplemental Data include five figures and additional Supplemental Experimental Procedures used in this work and are available with this article online at http://www.chembiol.com/cgi/content/full/15/1/51/DC1.

ACKNOWLEDGMENTS

We thank Albert Morrishow (Weill Medical College) and Dr. George Sukenick, Hui Fang, Hui Liu, and Sylvi Rusli (Memorial Sloan-Kettering Cancer Center [MSKCC]) for mass spectral analyses. Generous financial support has been provided by the National Institutes of Health (grant AI069209 to L.E.N.Q.), Stavros S. Niarchos Foundation (L.E.N.Q.), NYSTAR Watson Investigator Program (D.S.T.), William Randolph Hearst Foundation (L.E.N.Q. and D.S.T.), William H. Goodwin and Alice Goodwin and the Commonwealth Foundation for Cancer Research (D.S.T.), and MSKCC Experimental Therapeutics Center (D.S.T.). L.E.N.Q. was responsible for designing the study, directing the project, and writing the manuscript. D.S.T. oversaw the synthetic aspects of the project. D.S.T., X.L., J.-S.R., J.A.F., K.L.S., and C.E.S. edited the manuscript. J.A.F. contributed to the experimental design and conducted the enzyme characterization and inhibition experiments. K.L.S. contributed to the experimental design and conducted the genetic analysis and PGL inhibition experiments. C.E.S. performed the MS analysis. X.L. and J.-S.R. developed and executed the synthesis of pHB-AMS.

Received: September 20, 2007
Revised: November 24, 2007
Accepted: November 29, 2007
Published online: December 27, 2007

REFERENCES

Admiraal, S.J., Walsh, C.T., and Khosla, C. (2001). The loading module of rifamycin synthetase is an adenylation-thiolation didomain with substrate tolerance for substituted benzoates. Biochemistry *40*, 6116–6123.

Agrawal, A., Pandit, L., Dalal, M., and Shetty, J.P. (2005). Neurological manifestations of Hansen's disease and their management. Clin. Neurol. Neurosurg. *107*, 445–454.

Alksne, L.E., and Projan, S.J. (2000). Bacterial virulence as a target for antimicrobial chemotherapy. Curr. Opin. Biotechnol. *11*, 625–636.

Azad, A.K., Sirakova, T.D., Fernandes, N.D., and Kolattukudy, P.E. (1997). Gene knockout reveals a novel gene cluster for the synthesis of a class of cell wall lipids unique to pathogenic mycobacteria. J. Biol. Chem. *272*, 16741–16745.

Aziz, M.A., Wright, A., Laszlo, A., De Muynck, A., Portaels, F., Van Deun, A., Wells, C., Nunn, P., Blanc, L., and Raviglione, M. (2006). Epidemiology of antituberculosis drug resistance (the Global Project on Anti-tuberculosis Drug Resistance Surveillance): an updated analysis. Lancet *368*, 2142–2154.

Beuerle, T., and Pichersky, E. (2002). Enzymatic synthesis and purification of aromatic coenzyme a esters. Anal. Biochem. *302*, 305–312.

Britton, W.J., and Lockwood, D.N. (2004). Leprosy. Lancet *363*, 1209–1219.

Brown, B.A., Cain, M., Broadbent, J., Tompkins, S., Henrich, G., Joseph, R., Casto, S., Harney, H., Greene, R., Delmondo, R., et al. (1997). FlashPlate technology. In High Throughput Screening: the Discovery of Bioactive Substances, J.P. Devlin, ed. (New York: Marcel Dekker, Inc.), pp. 317–328.

Camacho, L.R., Ensergueix, D., Perez, E., Gicquel, B., and Guilhot, C. (1999). Identification of a virulence gene cluster of *Mycobacterium tuberculosis* by signature-tagged transposon mutagenesis. Mol. Microbiol. *34*, 257–267.

Centers for Disease Control and Prevention (2006). Emergence of *Mycobacterium tuberculosis* with extensive resistance to second-line drugs—worldwide, 2000–2004. MMWR Morb. Mortal. Wkly. Rep. *55*, 301–305.

Clatworthy, A.E., Pierson, E., and Hung, D.T. (2007). Targeting virulence: a new paradigm for antimicrobial therapy. Nat. Chem. Biol. *3*, 541–548.

Collins, D.M., Skou, B., White, S., Bassett, S., Collins, L., For, R., Hurr, K., Hotter, G., and de Lisle, G.W. (2005). Generation of attenuated *Mycobacterium bovis* strains by signature-tagged mutagenesis for discovery of novel vaccine candidates. Infect. Immun. *73*, 2379–2386.

Constant, P., Perez, E., Malaga, W., Laneelle, M.A., Saurel, O., Daffe, M., and Guilhot, C. (2002). Role of the *pks15/1* gene in the biosynthesis of phenolglycolipids in the *M. tuberculosis* complex: evidence that all strains synthesize glycosylated *p*-hydroxybenzoic methyl esters and that strains devoid of phenolglycolipids harbor a frameshift mutation in the *pks15/1* gene. J. Biol. Chem. *277*, 38148–38158.

Copeland, R.A. (2000). Tight binding inhibitors. In Enzymes: A Practical Introduction to Structure, Mechanism, and Data Analysis (New York: Wiley-VCH, Inc. Publications), pp. 305–317.

Cox, J.S., Chen, B., McNeil, M., and Jacobs, W.R., Jr. (1999). Complex lipid determines tissue-specific replication of *Mycobacterium tuberculosis* in mice. Nature *402*, 79–83.

Daffe, M., and Draper, P. (1998). The envelope layers of mycobacteria with reference to their pathogenicity. Adv. Microb. Physiol. *39*, 131–203.

Ferreras, J.A., Ryu, J.S., Di Lello, F., Tan, D.S., and Quadri, L.E. (2005). Small-molecule inhibition of siderophore biosynthesis in *Mycobacterium tuberculosis* and *Yersinia pestis*. Nat. Chem. Biol. *1*, 29–32.

Fischbach, M.A., and Walsh, C.T. (2006). Assembly-line enzymology for polyketide and nonribosomal peptide antibiotics: logic, machinery, and mechanisms. Chem. Rev. *106*, 3468–3496.

Katoch, V.M. (2004). Infections due to non-tuberculous mycobacteria (NTM). Indian J. Med. Res. *120*, 290–304.

Kim, S., Lee, S.W., Choi, E.C., and Choi, S.Y. (2003). Aminoacyl-tRNA synthetases and their inhibitors as a novel family of antibiotics. Appl. Microbiol. Biotechnol. *61*, 278–288.

Kolattukudy, P.E., Fernandes, N.D., Azad, A.K., Fitzmaurice, A.M., and Sirakova, T.D. (1997). Biochemistry and molecular genetics of cell-wall lipid biosynthesis in mycobacteria. Mol. Microbiol. *24*, 263–270.

Larimer, F.W., Chain, P., Hauser, L., Lamerdin, J., Malfatti, S., Do, L., Land, M.L., Pelletier, D.A., Beatty, J.T., Lang, A.S., et al. (2004). Complete genome sequence of the metabolically versatile photosynthetic bacterium *Rhodopseudomonas palustris*. Nat. Biotechnol. *22*, 55–61.

Maeda, S., Matsuoka, M., Nakata, N., Kai, M., Maeda, Y., Hashimoto, K., Kimura, H., Kobayashi, K., and Kashiwabara, Y. (2001). Multidrug resistant *Mycobacterium leprae* from patients with leprosy. Antimicrob. Agents Chemother. *45*, 3635–3639.

Marra, A. (2004). Can virulence factors be viable antibacterial targets? Expert Rev. Anti Infect. Ther. *2*, 61–72.

Matsuoka, M., Kashiwabara, Y., Liangfen, Z., Goto, M., and Kitajima, S. (2003). A second case of multidrug-resistant *Mycobacterium leprae* isolated from a Japanese patient with relapsed lepromatous leprosy. Int. J. Lepr. Other Mycobact. Dis. *71*, 240–243.

May, J.J., Kessler, N., Marahiel, M.A., and Stubbs, M.T. (2002). Crystal structure of DhbE, an archetype for aryl acid activating domains of modular nonribosomal peptide synthetases. Proc. Natl. Acad. Sci. USA *99*, 12120–12125.

Miethke, M., Bisseret, P., Beckering, C.L., Vignard, D., Eustache, J., and Marahiel, M.A. (2006). Inhibition of aryl acid adenylation domains involved in bacterial siderophore synthesis. FEBS J. *273*, 409–419.

Minnikin, D.E., Kremer, L., Dover, L.G., and Besra, G.S. (2002). The methyl-branched fortifications of *Mycobacterium tuberculosis*. Chem. Biol. *9*, 545–553.

Moore, B.S., and Hertweck, C. (2002). Biosynthesis and attachment of novel bacterial polyketide synthase starter units. Nat. Prod. Rep. *19*, 70–99.

Ng, V., Zanazzi, G., Timpl, R., Talts, J.F., Salzer, J.L., Brennan, P.J., and Rambukkana, A. (2000). Role of the cell wall phenolic glycolipid-1 in the peripheral nerve predilection of *Mycobacterium leprae*. Cell *103*, 511–524.

Niu, G., Liu, G., Tian, Y., and Tan, H. (2006). SanJ, an ATP-dependent picolinate-CoA ligase, catalyzes the conversion of picolinate to picolinate-CoA during nikkomycin biosynthesis in *Streptomyces ansochromogenes*. Metab. Eng. *8*, 183–195.

Norris, A.T., and Berg, P. (1964). Mechanism of aminoacyl RNA synthesis: studies with isolated aminoacyl adenylate complexes of isoleucyl RNA synthetase. Proc. Natl. Acad. Sci. USA *52*, 330–337.

Onwueme, K.C., Ferreras, J.A., Buglino, J., Lima, C.D., and Quadri, L.E. (2004). Mycobacterial polyketide-associated proteins are acyltransferases: proof of principle with *Mycobacterium tuberculosis* PapA5. Proc. Natl. Acad. Sci. USA *101*, 4608–4613.

Onwueme, K.C., Vos, C.J., Zurita, J., Ferreras, J.A., and Quadri, L.E. (2005a). The dimycocerosate ester polyketide virulence factors of mycobacteria. Prog. Lipid Res. *19*, 259–302.

Onwueme, K.C., Vos, C.J., Zurita, J., Soll, C.E., and Quadri, L.E. (2005b). Identification of phthiodiolone ketoreductase, an enzyme required for production of mycobacterial diacyl phthiocerol virulence factors. J. Bacteriol. *187*, 4760–4766.

Papa, F., Riviere, M., Fournie, J.J., Puzo, G., and David, H. (1987). Specificity of a *Mycobacterium kansasii* phenolic glycolipid (mycoside A) immunoserum. J. Clin. Microbiol. *25*, 2270–2273.

Parish, T., and Stoker, N.G. (2000). Use of a flexible cassette method to generate a double unmarked *Mycobacterium tuberculosis tlyA plcABC* mutant by gene replacement. Microbiology *146*, 1969–1975.

Perez, E., Constant, P., Laval, F., Lemassu, A., Laneelle, M.A., Daffe, M., and Guilhot, C. (2004). Molecular dissection of the role of two methyltransferases in the biosynthesis of phenolglycolipids and phthiocerol dimycocerosate in the *Mycobacterium tuberculosis* complex. J. Biol. Chem. *279*, 42584–42592.

Quadri, L.E.N. (2007). Strategic paradigm shifts in the antimicrobial drug discovery process of the 21st century. Infect. Disord. Drug Targets *7*, 230–237.

Quadri, L.E.N., Sello, J., Keating, T.A., Weinreb, P.H., and Walsh, C.T. (1998a). Identification of a *Mycobacterium tuberculosis* gene cluster encoding the biosynthetic enzymes for assembly of the virulence-conferring siderophore mycobactin. Chem. Biol. *5*, 631–645.

Quadri, L.E.N., Weinreb, P.H., Lei, M., Nakano, M.M., Zuber, P., and Walsh, C.T. (1998b). Characterization of Sfp, a *Bacillus subtilis* phosphopantetheinyl transferase for peptidyl carrier protein domains in peptide synthetases. Biochemistry *37*, 1585–1595.

Rambukkana, A., Zanazzi, G., Tapinos, N., and Salzer, J.L. (2002). Contact-dependent demyelination by *Mycobacterium leprae* in the absence of immune cells. Science *296*, 927–931.

Reed, M.B., Domenech, P., Manca, C., Su, H., Barczak, A.K., Kreiswirth, B.N., Kaplan, G., and Barry, C.E., 3rd. (2004). A glycolipid of hypervirulent tuberculosis strains that inhibits the innate immune response. Nature *431*, 84–87.

Ruley, K.M., Ansede, J.H., Pritchett, C.L., Talaat, A.M., Reimschuessel, R., and Trucksis, M. (2004). Identification of *Mycobacterium marinum* virulence genes using signature-tagged mutagenesis and the goldfish model of mycobacterial pathogenesis. FEMS Microbiol. Lett. *232*, 75–81.

Simeone, R., Constant, P., Guilhot, C., Daffe, M., and Chalut, C. (2007a). Identification of the missing *trans*-acting enoyl reductase required for phthiocerol dimycocerosate and phenolglycolipid biosynthesis in *Mycobacterium tuberculosis*. J. Bacteriol. *189*, 4597–4602.

Simeone, R., Constant, P., Malaga, W., Guilhot, C., Daffe, M., and Chalut, C. (2007b). Molecular dissection of the biosynthetic relationship between phthiocerol and phthiodiolone dimycocerosates and their critical role in the virulence and permeability of *Mycobacterium tuberculosis*. FEBS J. *274*, 1957–1969.

Somu, R.V., Boshoff, H., Qiao, C., Bennett, E.M., Barry Iii, C.E., and Aldrich, C.C. (2006). Rationally designed nucleoside antibiotics that inhibit siderophore biosynthesis of *Mycobacterium tuberculosis*. J. Med. Chem. *49*, 31–34.

Stadthagen, G., Kordulakova, J., Griffin, R., Constant, P., Bottova, I., Barilone, N., Gicquel, B., Daffe, M., and Jackson, M. (2005). *p*-Hydroxybenzoic acid synthesis in *Mycobacterium tuberculosis*. J. Biol. Chem. *280*, 40699–40706.

Stinear, T.P., Seemann, T., Pidot, S., Frigui, W., Reysset, G., Garnier, T., Meurice, G., Simon, D., Bouchier, C., Ma, L., et al. (2007). Reductive evolution and niche adaptation inferred from the genome of *Mycobacterium ulcerans*, the causative agent of Buruli ulcer. Genome Res. *17*, 192–200.

Triccas, J.A., Parish, T., Britton, W.J., and Gicquel, B. (1998). An inducible expression system permitting the efficient purification of a recombinant antigen from *Mycobacterium smegmatis*. FEMS Microbiol. Lett. *167*, 151–156.

Trivedi, O.A., Arora, P., Sridharan, V., Tickoo, R., Mohanty, D., and Gokhale, R.S. (2004). Enzymic activation and transfer of fatty acids as acyl-adenylates in mycobacteria. Nature *428*, 441–445.

Trivedi, O.A., Arora, P., Vats, A., Ansari, M.Z., Tickoo, R., Sridharan, V., Mohanty, D., and Gokhale, R.S. (2005). Dissecting the mechanism and assembly of a complex virulence mycobacterial lipid. Mol. Cell *17*, 631–643.

Tsenova, L., Ellison, E., Harbacheuski, R., Moreira, A.L., Kurepina, N., Reed, M.B., Mathema, B., Barry, C.E., 3rd, and Kaplan, G. (2005). Virulence of selected *Mycobacterium tuberculosis* clinical isolates in the rabbit model of meningitis is dependent on phenolic glycolipid produced by the bacilli. J. Infect. Dis. *192*, 98–106.

Velayati, A.A., Boloorsaze, M.R., Farnia, P., Mohammadi, F., Karam, M.B., and Masjedi, M.R. (2005). *Mycobacterium gastri* causing disseminated infection in children of same family. Pediatr. Pulmonol. *39*, 284–287.

Webster, L.T., Jr. (1963). Studies of the acetyl coenzyme a synthetase reaction. I. Isolation and characterization of enzyme-bound acetyl adenylate. J. Biol. Chem. *238*, 4010–4015.

World Health Organization. (2007a). Tuberculosis (http://www.who.int/mediacentre/factsheets/fs104/en/print.html).

World Health Organization. (2007b). Leprosy (http://www.who.int/mediacentre/factsheets/fs101/en/).